Science and Technology Facilities Council

Technical Report
STFC-TR-2026-010

# Benchmarking SASfit Hankel transform strategies

J Huntley, L Protopapa, J Kohlbrecher

March 2026

Enquiries concerning this report should be addressed to:

RAL Library
STFC Rutherford Appleton Laboratory
Harwell Oxford
Didcot
OX11 0QX

Tel: +44(0)1235 445577
email: library@stfc.ac.uk

Science and Technology Facilities Council reports are available online at:
https://epubs.stfc.ac.uk

Accessibility: a Microsoft Word version of this document (for use with assistive technology) may be available on request.

**DOI: 10.5286/stfctr.2026010**

**ISSN 2753-5797**

## STFC Author Identifiers (ORCIDs)

Author ORCIDs are provided where available.


| | |
|---|---|
| Jessica Huntley | 0009-0008-7651-6149 |
| Letizia Protopapa | 0009-0008-6781-5876 |
| Joachim Kohlbrecher | 0000-0001-5879-6943 |

# Benchmarking SASfit Hankel Transform Strategies

Jessica Huntley[a] , Letizia Protopapa[a] , Joachim Kohlbrecher[b]
[a] Science and Technology Facilities Council, Rutherford Appleton Laboratory,
Harwell Campus, Didcot, OX11 0QX
[b] Laboratory for Neutron Scattering and Imaging,
Paul Scherrer Institute, Villigen, CH-5232, Switzerland

March 31, 2026

## 1 Introduction

The Hankel transform, also known as the Fourier–Bessel transform, is widely used in the analysis of small angle scattering (SAS) data. The transform is needed in many areas, e.g. to calculate scattering functions, to correct for multiple scattering, to simulate spin echo signals like those obtained on Larmor at the ISIS Neutron and Muon Source, as well as to qualitatively analyse phase contrast images (PCI) taken at the Diamond synchrotron source.

SAS is an experimental technique using X-rays (SAXS) or neutrons (SANS) to study the structure of materials on the nanoscale (roughly 1–1000 nm). SAS measures how radiation is scattered at very small angles, which tells us about large-scale structures inside the sample.

The setup of a SANS experiment is described by the following picture, taken from a paper by Jeffries et al. [7]:

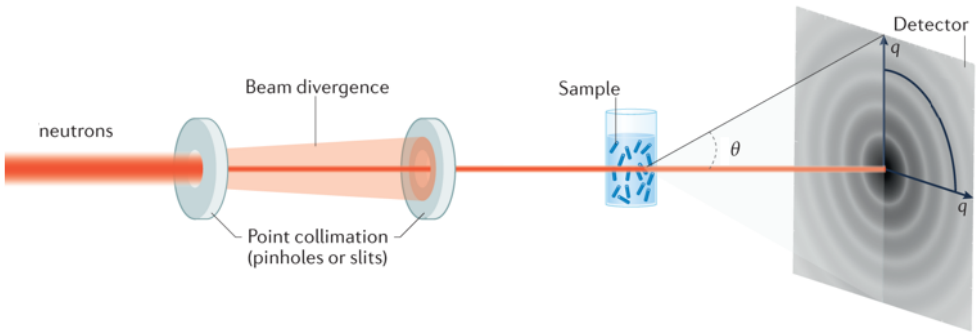


Figure 1: Example SAS setup [7].

A beam of neutrons is shone on a sample and, as the neutrons interact with the sample, the beam is scattered at small angles (represented by $\theta$ in Fig. 1). Scattered neutrons hit the detector, which measures the intensity $I(Q)$ of the scattered neutrons as a function of the scattering vector $Q$ [5].

The scattering vector $Q$ is a function of the scattering angle $\theta$ and is given by

$$Q = \frac{4\pi}{\lambda} \sin\left(\frac{\theta}{2}\right) \tag{1}$$

where $\lambda$ is the neutron wavelength. The scattering vector plays a crucial role in the computation of the Hankel transform, which has the following mathematical formulation:

$$I(Q) = \int_0^\infty G(r) J_\nu(Qr)\, r\, dr \tag{2}$$

where:

- $G(r)$ is the original function expressed in terms of the radial coordinate $r$ in physical space. The function is assumed to be radially symmetric, so it depends only on the distance from the origin.
- $r$ is the radial coordinate in real (physical) space.
- $Q$ is the radial spatial frequency (also called the transverse wavenumber). It is the conjugate variable of $r$, playing the same role as the angular frequency in the Fourier transform.
- $J_\nu(Qr)$ is the Bessel function of the first kind of order $\nu$. It acts as the kernel of the transform and replaces the exponential kernel of the Fourier transform when cylindrical symmetry is present.
- $\nu$ is the order of the Hankel transform. The most common case is $\nu = 0$, corresponding to circular symmetry without angular dependence.
- $I(Q)$ is the transformed function in radial frequency space. It describes how the original function $G(r)$ is distributed over radial spatial frequencies.

Conveniently, the Hankel transform is its own inverse, so that:

$$G(r) = \int_0^\infty I(Q) J_\nu(Qr)\, Q\, dQ \tag{3}$$

The transformation over the oscillating Bessel function makes this kind of integral unsuitable or inefficient for standard integration routines. Furthermore, the oscillations of the Bessel functions are not strictly periodic, so strategies for solving Fourier integrals cannot be directly used. In this work we have started to compare the precision as well as speed of some commonly used strategies for Hankel transform with emphasis on a class of functions used in small angle scattering.

## 2 Hankel Transform Strategies

SASfit [2] is a software package for fitting SAS curves. In SASfit, there are currently 15 different implementations of the Hankel transform, i.e., 15 different ways of approximating the Hankel transform integral. In Table 1, we report their names, characteristics, and the paper from which they have been taken. The strategies are numbered for simplicity, as from now on we will refer to them through that number.

As can be seen in the table, strategies 6-11 rely on digital filters and compute the Hankel transform through a fixed grid. They differ mainly in the way the filter is designed and for the number of nodes. When using these strategies, the user has no way to control the accuracy of the result. Furthermore, these strategies are designed for first- and second order Hankel transforms, whereas the others do not have this limitation. On the other hand, strategies 0, 5, 12 and 13 require the user to supply a parameter that corresponds to the relative error allowed. Both strategies 0 and 1 rely on a double-exponential quadrature approach, although strategy 1 is developed specifically for Bessel functions and does not require a relative-error parameter (unlike strategy 0 which has been developed for periodic oscillating functions). Strategies 2-4 require some knowledge regarding the shape of the scattering function.

| index | Strategy name | Characteristics | ref. |
|---|---|---|---|
| 0 | OOURA_DEO | Double-exponential quadrature, with rel. error-control | [12] |
| 1 | OGATA_2005 | Double-exponential quadrature (for bessel func.) | [11] |
| 2 | FBT0 | Requires knowledge of function | [8] |
| 3 | FBT1 | Requires knowledge of function | [8] |
| 4 | FBT2 | Requires knowledge of function | [8] |
| 5 | GSL_QAWF | With rel. error-control | [4, 14][1] |
| 6 | GUPTASARMA_97 | Digital filter, fixed-grid | [6] |
| 7 | GUPTASARMA_97_FAST | Digital filter, fixed-grid | [6] |
| 8 | KEY_51 | Digital filter, fixed-grid | [10, 13] |
| 9 | KEY_101 | Digital filter, fixed-grid | [10, 13] |
| 10 | KEY_201 | Digital filter, fixed-grid | [10, 13] |
| 11 | ANDERSON_801 | Digital filter, fixed-grid | [1, 13] |
| 12 | QWE | With rel. error-control | [9, 13] |
| 13 | CHAVE | Automatic integration, with rel. error-control | [1] |
| 14 | SINC_SEO | Automatic integration, with abs. error-control | [3] |

Table 1: Hankel transform strategies available in SASfit as well as their characteristics and references to respective papers.

# 3 Test functions

We tested strategies in Table 1, on various form factor functions, having different characteristics as well as an analytical solution for the Hankel transform to easily check the numerical precision. The chosen form factors are:

1. `gDAB:`
   strictly monotonic decaying
2. `Broad-Peak:`
   function with a peak at a certain $q$-value, whereas the peak width can be controlled by another parameter $\xi$
3. `sphere:`
   fast oscillating function

For the broad-peak function, we computed results for three values of $\xi$, specifically 100, 500, 1000.

In Figure 2, we show the original scattering function and the corresponding Spin-Echo Small-Angle Neutron Scattering (SESANS) signal for each of: gDAB, sphere, broad-peak with $\xi$=100 and broad-peak with $\xi$=1000. For each value on the $x$ axis, the SESANS signal $G_{\mathrm{SESANS}}(x)$ is computed as the difference between the Hankel transform of the scattering function computed at $x$, and the Hankel transform of the scattering function computed at 0, i.e.

$$G_{\mathrm{SESANS}}(x) = \frac{1}{2\pi}\left(G(x) - G(0)\right) \tag{4}$$

using eq. 3 with $I(Q)$ being one of the above mentioned form factors.

[1] This option tries to use the cos-Fourier integral from gsl and is therefore feeding `gsl_integration_qawf` with the function $QI(Q)J_0(Qr' + \phi_0)/\cos(Qr')$ with $\phi_0 = \frac{\pi}{4}(1 + 2\nu)$ after the variable transform $r = r' + \phi_0/Q$ as $J_\nu(x) = \sqrt{\frac{2}{\pi x}}\cos\left(x - \frac{\nu\pi}{2} - \frac{\pi}{4}\right)$ for $x \gg 1$

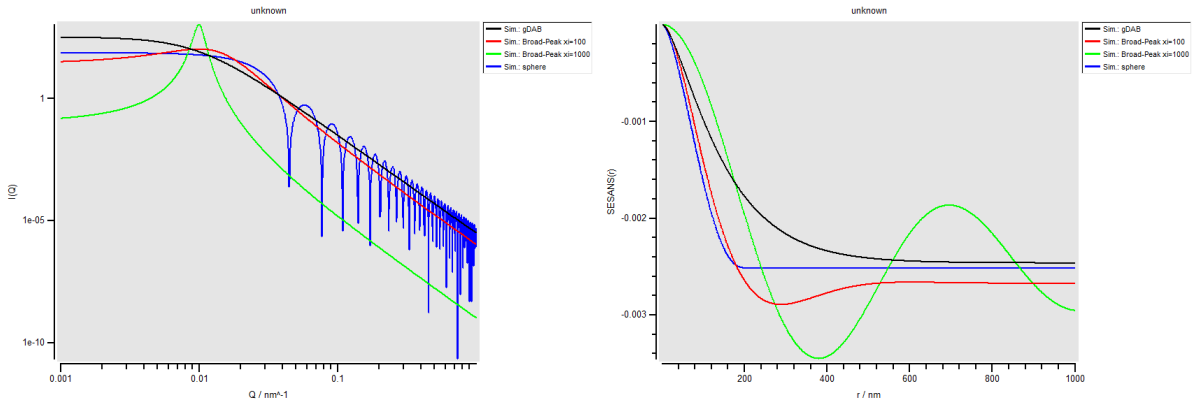


Figure 2: Scattering function (left) and corresponding SESANS signal (right), which is basically the Hankel transform of the scattering function.

From Figure 2, it is possible to see how the peak of the broad-peak function gets emphasized when $\xi$ changes from 100 to 1000 (left plot, colours green and red), as well as the corresponding oscillation in the SESANS signal (right plot).

# 4 Results

To measure the accuracy of the results we use the normalised root mean squared error (NRMSE), computed between the obtained result and the analytical solution, as follows:

$$\text{NRMSE} = \frac{\text{RMSE}}{\max(\hat{y}) - \min(\hat{y})} \tag{5}$$

where $y$ is the actual solution and $\hat{y}$ is the predicted solution, and RMSE is computed as:

$$\text{RMSE} = \sqrt{\frac{1}{n}\sum_{i=1}^{n}(y_i - \hat{y}_i)^2} \tag{6}$$

In Figures 3 and 4, we show runtimes and NRMSEs for each of the strategies listed in Table 1 for different form factor functions.

For each form factor (that is, for each row) results are colour-coded from green to red, with green indicating best performance and red worst.

| Form Factor | Strategy | | | | | | | | | | | | | | |
|---|---|---|---|---|---|---|---|---|---|---|---|---|---|---|---|
| | 0 | 1 | 2 | 3 | 4 | 5 | 6 | 7 | 8 | 9 | 10 | 11 | 12 | 13 | 14 |
| gDAB | 1.29E-02 | 3.76E-02 | 2.64E-02 | 2.51E-02 | 2.48E-02 | 2.94E-01 | 1.01E-02 | 5.62E-03 | 5.05E-03 | 8.29E-03 | 1.53E-02 | 5.91E-02 | 7.96E-02 | 7.80E-02 | 7.40E-03 |
| Broad Peak, ξ=100 | 2.64E-02 | 3.93E-02 | 2.60E-02 | 2.23E-02 | 2.42E-02 | 4.85E-01 | 8.90E-03 | 4.86E-03 | 4.15E-03 | 8.06E-03 | 1.42E-02 | 5.68E-02 | 5.20E-02 | 4.96E-02 | 8.47E-03 |
| Broad Peak, ξ=500 | 7.06E-02 | 4.23E-02 | 2.99E-02 | 2.64E-02 | 2.56E-02 | 3.51E-01 | 1.04E-02 | 6.03E-03 | 5.46E-03 | 9.63E-03 | 1.74E-02 | 6.14E-02 | 8.25E-02 | 7.35E-02 | 3.82E-03 |
| Broad Peak, ξ=1000 | 1.35E-01 | 4.22E-02 | 2.84E-02 | 2.51E-02 | 2.65E-02 | 2.49E-01 | 1.03E-02 | 5.71E-03 | 5.13E-03 | 8.97E-03 | 1.65E-02 | 6.22E-02 | 7.16E-02 | 6.78E-02 | 3.74E-03 |
| Spheres | 4.94E-02 | 4.59E-02 | 3.25E-02 | 2.89E-02 | 2.92E-02 | 6.73E+00 | 1.16E-02 | 6.23E-03 | 5.32E-03 | 9.89E-03 | 1.79E-02 | 7.22E-02 | 5.25E-01 | 5.19E-01 | 7.04E-03 |

Figure 3: Runtimes for all strategies and form factors

| Form Factor | Strategy | | | | | | | | | | | | | | |
|---|---|---|---|---|---|---|---|---|---|---|---|---|---|---|---|
| | 0 | 1 | 2 | 3 | 4 | 5 | 6 | 7 | 8 | 9 | 10 | 11 | 12 | 13 | 14 |
| gDAB | 2.33E-12 | 1.24E-05 | 2.41E-04 | 1.89E-04 | 4.90E-04 | 1.11E-08 | 5.25E-12 | 1.74E-09 | 3.80E-08 | 2.48E-11 | 1.87E-14 | 2.78E-09 | 1.98E-10 | 1.99E-10 | 1.85E-05 |
| Broad Peak, ξ=100 | 1.19E-02 | 1.19E-02 | 1.19E-02 | 1.23E-02 | 3.40E-01 | 1.19E-02 | 1.19E-02 | 1.19E-02 | 1.19E-02 | 1.19E-02 | 1.19E-02 | 1.19E-02 | 1.19E-02 | 1.19E-02 | 1.19E-02 |
| Broad Peak, ξ=500 | 2.79E-03 | 2.78E-03 | 2.79E-03 | 2.79E-03 | 3.51E-01 | 2.79E-03 | 1.16E-02 | 3.45E-02 | 3.50E-02 | 1.47E-01 | 2.87E-03 | 2.78E-03 | 2.79E-03 | 2.79E-03 | 5.00E-03 |
| Broad Peak, ξ=1000 | 2.76E-03 | 3.56E-03 | 2.79E-03 | 3.37E-03 | 3.80E-01 | 2.76E-03 | 1.17E-01 | 1.87E-01 | 1.32E-01 | 7.19E-01 | 2.26E-02 | 7.12E-03 | 2.76E-03 | 2.76E-03 | 7.01E-02 |
| Spheres | 8.16E-04 | 8.17E-04 | 8.27E-04 | 8.28E-04 | 1.29E-01 | 8.17E-04 | 1.07E-03 | 1.75E-03 | 1.27E-03 | 1.14E-03 | 8.41E-04 | 8.36E-04 | 8.17E-04 | 8.17E-04 | 1.06E-03 |

Figure 4: NRMSEs for all strategies and form factors

Strategy 5 is consistently the slowest, approximately 1200 times slower than fastest strategy for spheres, while strategy 4 is consistently the least accurate, independently of the form factor.

In general, all strategies (other than strategy 4) perform well for the $\xi$=500 broad-peak case, strategies 6-11 and 14 perform poorer relative to the most accurate strategies as $\xi$ increases.

Strategies 7, 8 and 14 are fast across all form factors, but less consistency across strategies in terms of accuracy with different best performing strategy for each form factor studied. Strategies, which are consistently amongst the most accurate are strategies 0, 5, 12, and 13.

## 4.1 Output of transforms

This section shows the SESANS signals for the various Hankel transform strategies (computed through Equation 4), for each form factor. In all figures, we also include the analytical SESANS signal for that form factor.

### 4.1.1 gDAB

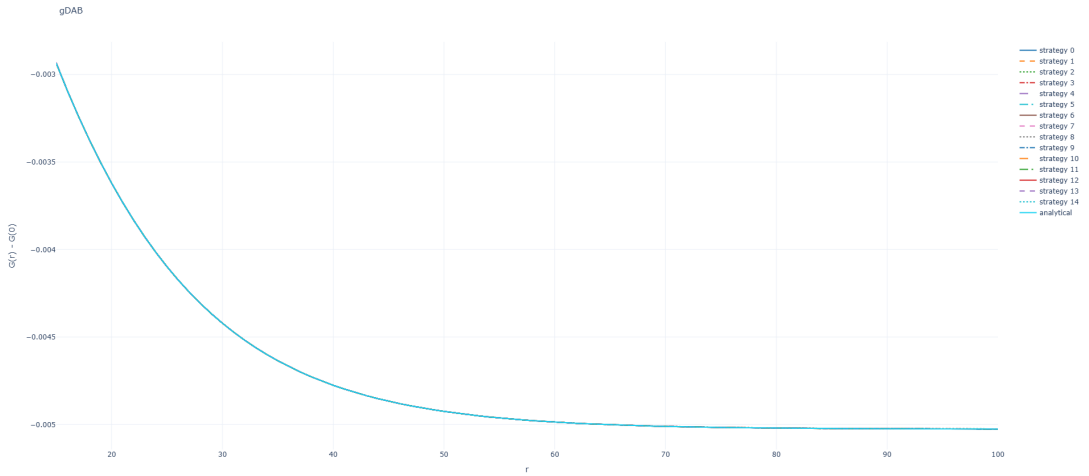


Figure 5: SESANS signal obtained through SASfit Hankel transform and analytical one, for gDAB, all strategies. Please note that the lines nicely overlap, which is the reason why only one color is visible.

### 4.1.2 Broad-peak

The plots in this subsection specifically refer to the broad-peak form factor, for the 3 different values of the $\xi$ parameter: 100, 500, 1000. Some plots show all strategies, while others focus on the best ones. When strategies have been hidden, this is visible from the legend on the right as they appear grayed out.

A few comments on the plots can be found after the pictures.

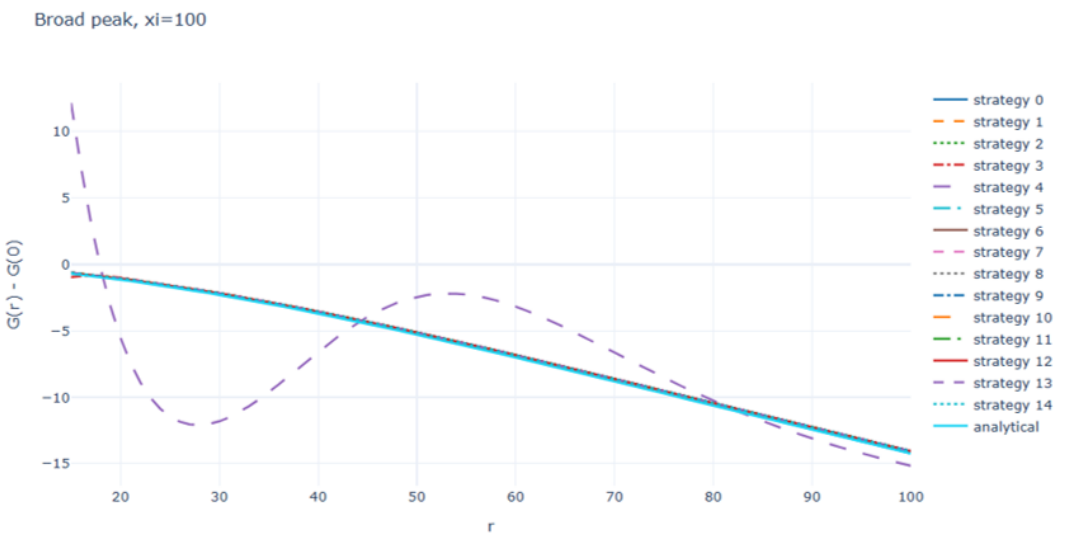


Figure 6: SESANS signal obtained through SASfit Hankel transform and analytical one, for broad-peak, $\xi$=100, all strategies.

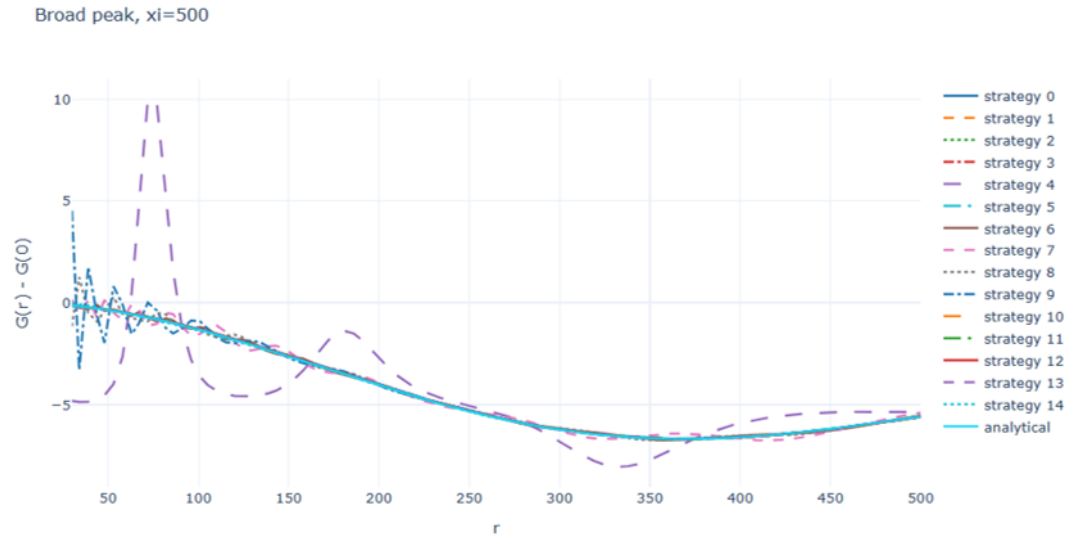


Figure 7: SESANS signal obtained through SASfit Hankel transform and analytical one, for broad-peak, $\xi$=500, all strategies.

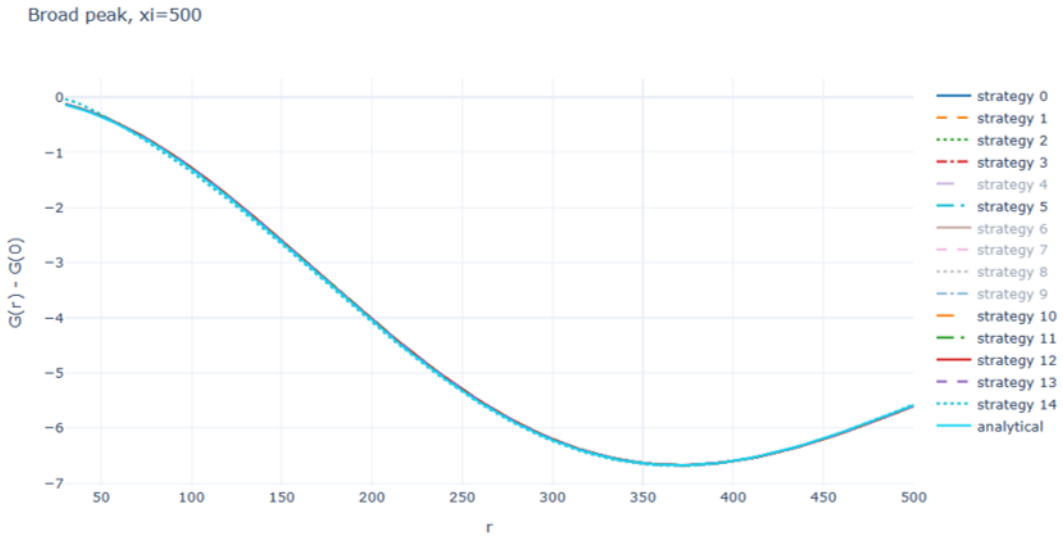


Figure 8: SESANS signal obtained through SASfit Hankel transform and analytical one, for broad-peak, $\xi$=500, best strategies.

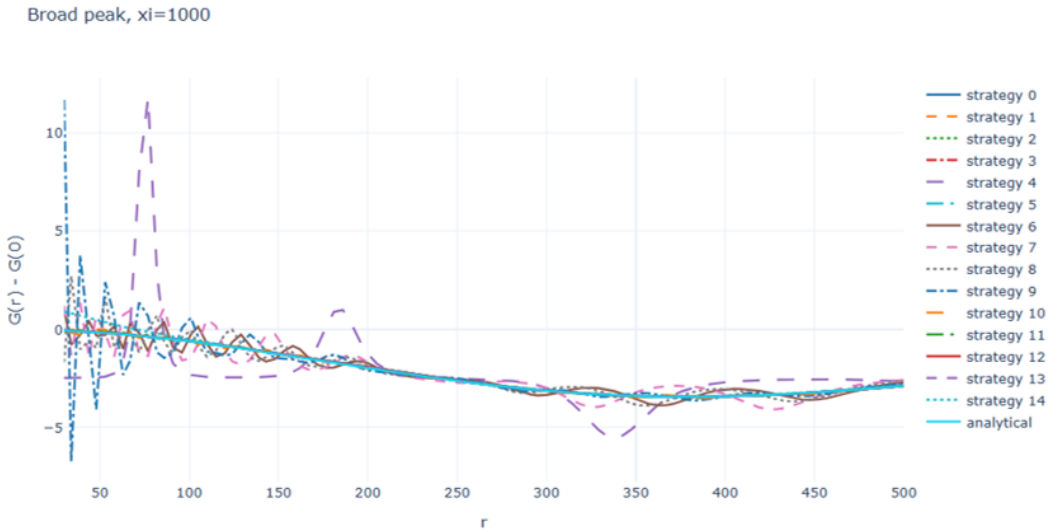


Figure 9: SESANS signal obtained through SASfit Hankel transform and analytical one, for broad-peak, $\xi$=1000, all strategies.

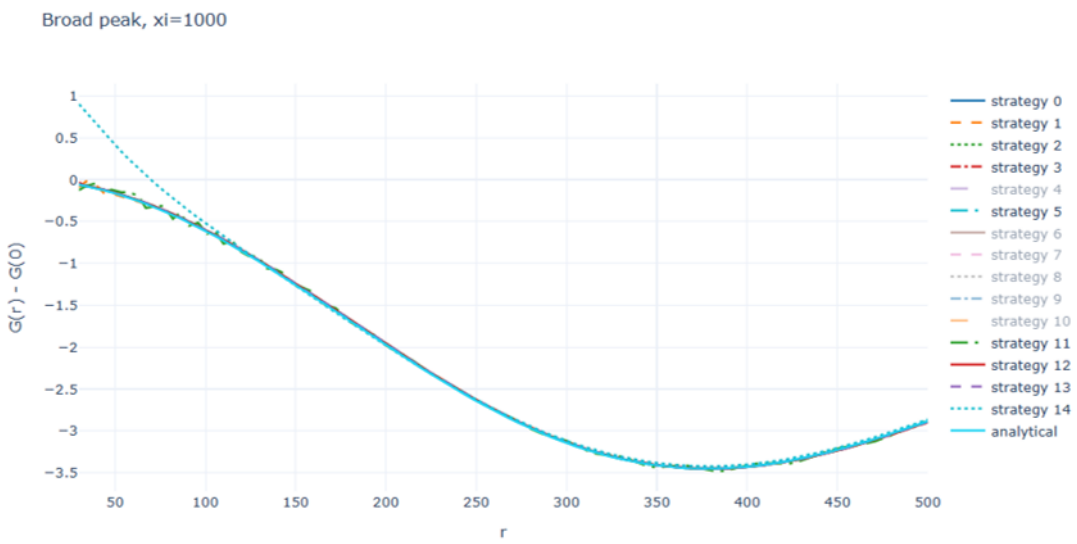


Figure 10: SESANS signal obtained through SASfit Hankel transform and analytical one, for broad-peak, $\xi$=1000, best strategies.

Strategy 4 performs badly with broad-peak, independently of the input parameters.

Strategies 6 to 11, that is, the fixed-grid ones, perform fine on small $\xi$, but poorly for larger $\xi$.

Strategies 1, 3, and 14 have their performance very much affected by the parameter "h ogata" (for the first two) and "eps nriq" (for the last), where "h ogata" indicates the point at which the form factor has a maximum and "eps nriq" is the error allowed. Tweaking these parameters allowed these strategies to perform quite well even for larger $\xi$. For smaller $\xi$, tweaking didn't seem as necessary.

### 4.1.3 Spheres

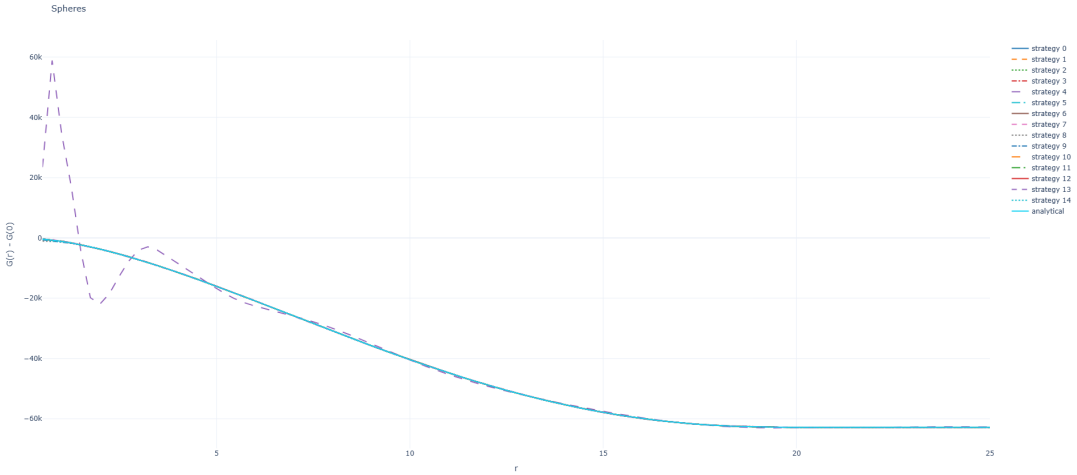


Figure 11: SESANS signal obtained through SASfit Hankel transform and analytical one, for Spheres, all strategies.

## 4.2 RMSE vs runtimes

Here, we show some scatter plots that allow to compare the strategies in terms of accuracy and runtime. Each point in a plot represent a strategy, with its x and y coordinates representing relative runtime and rmse respectively. Points closer to the bottom-left corner corresponds to the strategies that are best when both runtime and accuracy are considered. Note that accuracy and runtime values shown for each

strategy are relative to all other strategies, as they have been normalised by the maximum (for each plot).

### 4.2.1 gDAB

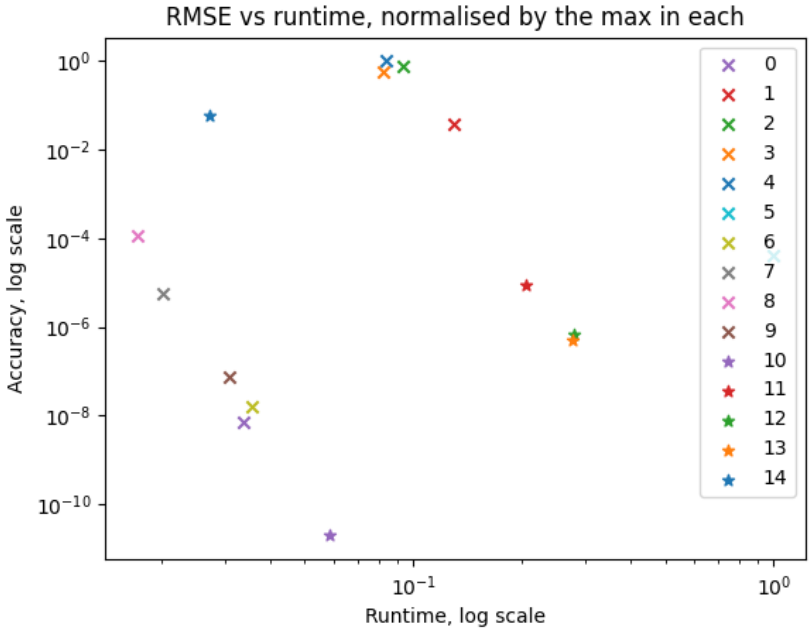


Figure 12: RMSE vs runtime for each strategy, for gDAB.

### 4.2.2 Broad-peak

The plots in this subsection specifically refer to the broad-peak form factor, for the 3 different values of the $\xi$ parameter: 100, 500, 1000.

We can see that strategy 5 is doing pretty badly compared to the others in terms of runtime, no matter $\xi$. For some other strategies, especially the non-error-controlled ones, the relative runtime increases with $\xi$.

Strategies 2 and 3, for which the input parameter h ogata has been optimised, are the ones doing best in terms of accuracy for the case $\xi = 1000$. They do pretty well also for smaller $\xi$, but for smaller $\xi$ other strategies (e.g., 10 and 14) can get similar accuracy in less time.

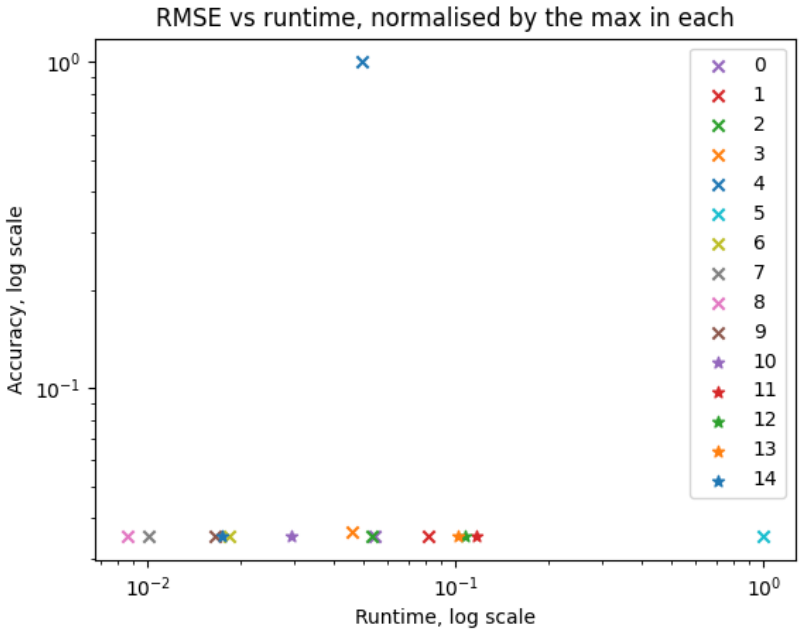


Figure 13: RMSE vs runtime for each strategy, for broad peak, $\xi$=100.

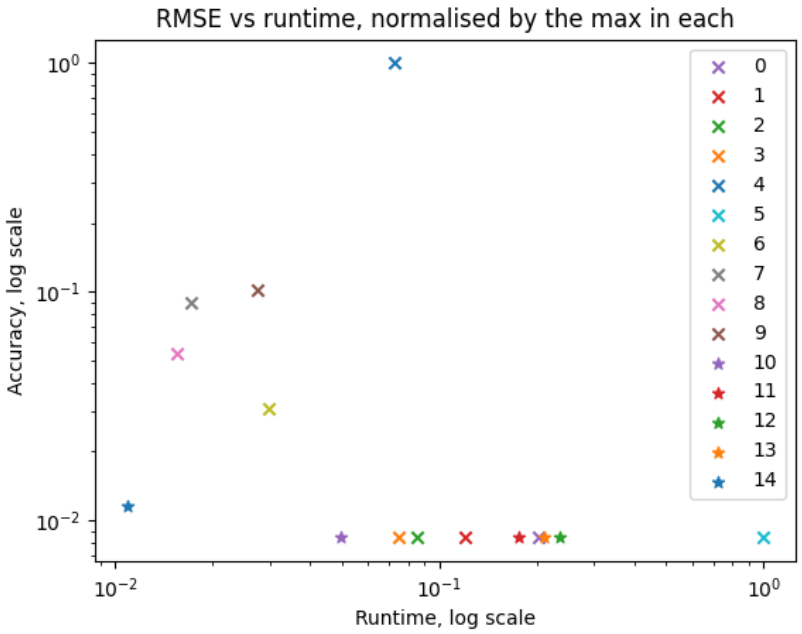


Figure 14: RMSE vs runtime for each strategy, for broad peak, $\xi$=500.

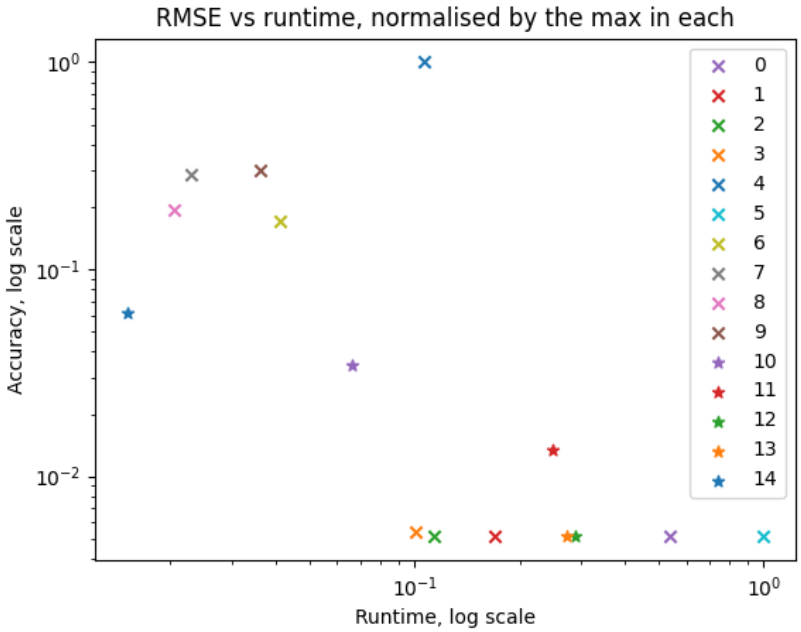


Figure 15: RMSE vs runtime for each strategy, for broad peak, $\xi$=1000.

#### 4.2.3 Spheres

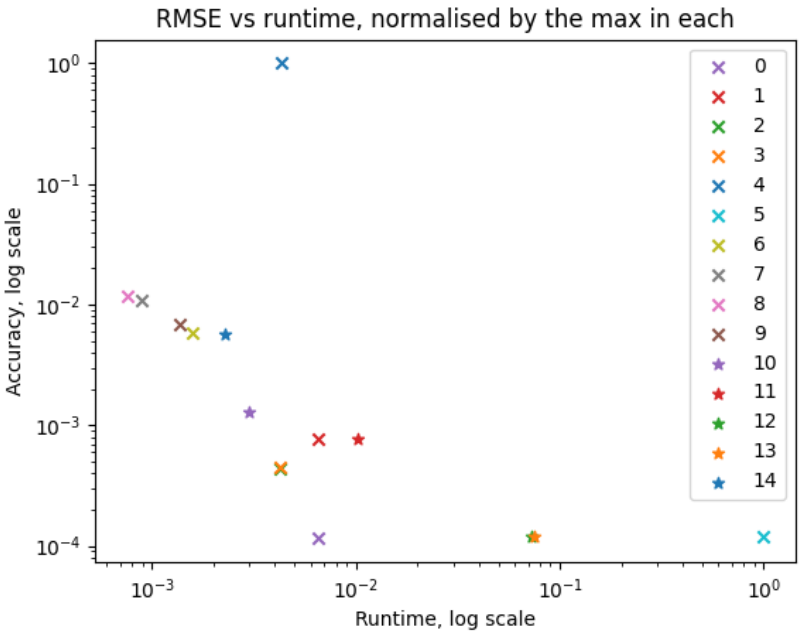


Figure 16: RMSE vs runtime for each strategy, for Spheres.

## 5 Conclusions

Our main conclusions are as follows:

- The quasi discrete Hankel transform (QDHT) strategies 6-11 (that is, the fixed-grid ones) are faster than others, but can become less accurate for complex form factors.

- The QDHT routines (6-11) can very easily be parallelized as it is a simple weighted sum over a fixed grid to speed up computations even more.
- Strategies 0, 12-14 are quite accurate even for complex form factors (oscillatory ones), but can take longer than fixed-grid ones.
- Therefore, when computing the Hankel transform on simple form factor functions (like gDAB) there is no need to use the error-control strategies, while for more complex functions it might be beneficial to start with any of strategies 6-11 and then refine the answer with the error-controlled ones. This information is particularly useful for the next stage of this work, which will consist in writing a C library specifically for computing Hankel transforms, by re-implementing the strategies available in SASfit and benchmarked here.
- For strategies 2-4, the user needs some knowledge of the form factor function, as these require a parameter corresponding to the point where the function $QI(Q)$ has a maximum.
- All strategies show increasing difficulties approaching $r \to 0$ and fail at $r = 0$, which is expected and called the quasi stationary case. At $r = 0$, other standard quadrature algorithms can be applied as supplied in many maths libraries.

# 6 Data access statement

Results and plots in this paper are generated with a set of Python scripts, which are available from the STFC Research Data Repository "eData" (https://doi.org/10.5286/edata/968). These scripts depend on SASfit, which is available under the GNU General Public Licence v3 from GitHub.

# References


[1] Walter L. Anderson. "Numerical integration of related Hankel transforms of orders 0 and 1 by adaptive digital filtering". In: *Geophysics* 47.12 (1982), pp. 1783–1798. ISSN: 0016-8033. DOI: 10.1190/1.1441448.

[2] Ingo Breßler, Joachim Kohlbrecher, and Andreas F. Thünemann. "*SASfit*: a tool for small-angle scattering data analysis using a library of analytical expressions". In: *Journal of Applied Crystallography* 48.5 (Oct. 2015), pp. 1587–1598. DOI: 10.1107/S1600576715016544. URL: https://doi.org/10.1107/S1600576715016544.

[3] Eleonora Denich and Paolo Novati. "A Sinc Rule for the Hankel Transform". In: *Journal of Scientific Computing* 100.1 (June 2024). ISSN: 1573-7691. DOI: 10.1007/s10915-024-02575-5.

[4] M. et al Galassi. *GNU Scientific Library Reference Manual (3rd Ed.)* ISBN: 0954612078. URL: https://www.gnu.org/software/gsl/.

[5] Cedric J. Gommes, Sebastian Jaksch, and Henrich Frielinghaus. "Small-angle scattering for beginners". In: *Journal of Applied Crystallography* 54.6 (2021), pp. 1832–1843. DOI: 10.1107/S1600576721010293.

[6] D. Guptasarma and B. Singh. "New digital linear filters for Hankel J0 and J1 transforms". In: *Geophysical Prospecting* 45.5 (1997), pp. 745–762. ISSN: 1365-2478. DOI: 10.1046/j.1365-2478.1997.500292.x.

[7] C. M. Jeffries, J. Ilavsky, A. Martel, et al. "Small-angle X-ray and neutron scattering". In: *Nature Reviews Methods Primers* 1.1 (2021), p. 70. DOI: 10.1038/s43586-021-00064-9.

[8] Zhong-Bo Kang et al. "Efficient Fourier transforms for transverse momentum dependent distributions". In: *Computer Physics Communications* 258 (2021), p. 107611. ISSN: 0010-4655. DOI: 10.1016/j.cpc.2020.107611.

[9] Kerry Key. "Is the fast Hankel transform faster than quadrature?" In: *Geophysics* 77.3 (2012), F21–F30. ISSN: 0016-8033. DOI: 10.1190/geo2011-0237.1.

[10] F. N. Kong. "Hankel transform filters for dipole antenna radiation in a conductive medium". In: *Geophysical Prospecting* 55.1 (2007), pp. 83–89. ISSN: 1365-2478. DOI: 10.1111/j.1365-2478.2006.00585.x.

[11] Hidenori Ogata. "A Numerical Integration Formula Based on the Bessel Functions". In: *Publications of the Research Institute for Mathematical Sciences* 41.4 (2005), pp. 949–970. ISSN: 0034-5318. DOI: 10.2977/PRIMS/1145474602.

[12] H. Takahasi and Masatake Mori. "The double exponential formula for oscillatory functions over the half infinite interval". In: *Journal of Computational and Applied Mathematics* 38.1–3 (1991), pp. 353–360. ISSN: 0377-0427. DOI: 10.1016/0377-0427(91)90181-I.

[13] Dieter Werthmüller. "An open-source full 3D electromagnetic modeler for 1D VTI media in Python: empymod". In: *Geophysics* 82.6 (2017), WB9–WB19. DOI: 10.1190/geo2016-0626.1. URL: https://doi.org/10.1190/geo2016-0626.1.

[14] Thomas Wieder. "Algorithm 794: numerical Hankel transform by the Fortran program HANKEL". In: *ACM Transactions on Mathematical Software* 25.2 (June 1999), pp. 240–250. ISSN: 0098-3500. DOI: 10.1145/317275.317284.